

# Hydrodynamic Self-Consistent Field Theory for Inhomogeneous Polymer Melts

David M. Hall,<sup>1,2</sup> Turab Lookman,<sup>2</sup> Glenn H. Fredrickson,<sup>3,4</sup> and Sanjy Banerjee<sup>4</sup>

<sup>1</sup> Department of Physics, University of California Santa Barbara, Santa Barbara, CA 93106

<sup>2</sup> Los Alamos National Laboratory, Theoretical Division, Los Alamos, NM 87545

<sup>3</sup> Materials Research Laboratory, University of California Santa Barbara, Santa Barbara, CA 93106

<sup>4</sup> Department of Chemical Engineering, University of California Santa Barbara, Santa Barbara, CA 93106

(dated: March 23, 2022)

We introduce a mesoscale technique for simulating the structure and rheology of block copolymer melts and blends in hydrodynamic flows. The technique couples dynamic self-consistent field theory (DSCFT) with continuum hydrodynamics and flow penalization to simulate polymeric fluids in channels of arbitrary geometry. We demonstrate the method by studying phase separation of an ABC triblock copolymer melt in a sub-micron channel with neutral wall wetting conditions. We find that surface wetting effects and shear effects compete, producing wall-perpendicular lamellae in the absence of flow, and wall-parallel lamellae in cases where the shear rate exceeds some critical Weissenberg number.

Predicting the non-equilibrium dynamics of multi-component inhomogeneous polymer formulations is important for development and improvement of paints, adhesives, cosmetics, and processed foods. Many such systems have fluid structures with length scales spanning nanometers to millimeters, and stabilization of the nest scale structures is often assisted by the presence of block or graft copolymers [1]. Computational tools which predict equilibrium properties of polymeric materials [2, 3] have been developed as a cost effective alternative to trial and error experimentation. However, bulk properties such as strength, optical clarity, and elasticity often depend in detail on the size and distribution of inhomogeneities in the system, which are determined both by the composition of the fluid and the manner in which it was processed.

We have developed a mesoscale technique aimed at examining the effects of hydrodynamic transport on polymer self assembly and viscoelasticity in industrial processing flows. The scheme couples dynamic self-consistent field theory (DSCFT) [4, 5, 6, 7] with a multiple-fluid Navier-Stokes system and a set of constitutive equations which describe viscoelastic stresses in a polymeric fluid. Both the thermodynamic and hydrodynamic portions of the model employ rigid wall fields which represent a slightly porous material that may be shaped to form channels with arbitrarily complex geometries. Each rigid object in the system may be fixed or moving, simulating the interaction of machine elements with polymers in the melt. We refer to the scheme as hydrodynamic self-consistent field theory (HSCFT) to underscore its emphasis on hydrodynamic transport.

In contrast to "phase field" techniques [8, 9, 10], this method simulates the assembly of multiblock copolymer mesophases where the polymeric nature of the chains is explicitly taken into account. It also differs from SCFT and DSCFT techniques in its ability to model hydrodynamic transport in complex channels with moving ma-

chinery. Generally speaking, SCFT is capable of describing equilibrium morphologies and micro-phases boundaries. DSCFT is capable of describing non-equilibrium systems in which hydrodynamic transport may be neglected, including phase separating melts and systems subjected to simple shear fields. HSCFT, in contrast, is appropriate for the description of non-equilibrium systems in which hydrodynamic effects play an important role including dynamic polymer nanocomposites, microfluidic channels, and micro-scale rheometry of material properties.

In this letter, we introduce a multi-fluid generalization of the "two-fluid" model of Doi and Onuki [11] followed by a summary of the thermodynamic equations used to model block-copolymer self assembly in the presence of rigid boundary surfaces. We illustrate the method by examining the effects of hydrodynamic transport on a phase separating triblock copolymer melt in a narrow channel.

In the most general case, the system is composed of a blend of  $C$  distinguishable copolymer species in a fixed volume,  $V$ . Each copolymer of species  $i$  is itself constructed from  $M_i$  distinct monomer types (such as polystyrene, polyethylene, etc.) Each copolymer species  $i$  is also taken to be monodisperse with a polymerization index  $N_i$  and an entanglement length  $N_e$ . In addition, the system contains a set of rigid walls which are constructed from  $M$  distinguishable solid materials.

We derive a hydrodynamic model for multiple viscoelastic fluids at low Reynolds number by employing the principles of irreversible thermodynamics as outlined in [11]. The method described therein consists of a formal procedure for constructing a Rayleigh functional  $R = \dot{F} + (1/2)W$  where  $\dot{F}$  represents the time derivative of the free energy and  $W$  is a dissipation functional. Extremizing  $R$  with respect to the component velocities produces hydrodynamic equations of motion while preserving the correct Onsager couplings. Due to space con-

straints, we present the results of the derivation here, deferring the details to a later publication.

The fluid composition at a given point  $r$  is described by monomer volume fractions  $\phi_{i1}(r)$  and wall volume fractions  $\phi_{j1}(r)$ . The first index on  $\phi_{i1}(r)$  indicates the copolymer species, and the second index indicates the material type (polystyrene, polyethylene, etc.) Note that in general, polystyrene monomers associated with one copolymer species  $\phi_{i1}(r)$  exhibit different dynamics from polystyrene monomers associated with a second copolymer species  $\phi_{i2}(r)$  requiring us to treat them as distinct fluids. The  $\phi_{j1}(r)$  indicates the volume fraction of solid material of type  $j$  at location  $r$ . By definition, all volume fractions sum to unity,  $\phi_{i1} + \phi_{j1} = 1$ . To save space, we employ the shorthand notation  $\phi_i = \sum_{i=1}^M \phi_{i1}$  and  $\phi_j = \sum_{j=1}^M \phi_{j1}$ .

In the absence of chemical reactions, the number density of each monomer species is conserved, as expressed by the continuity equations

$$\partial_t \phi_i + \nabla \cdot (\mathbf{v}_i \phi_i) = 0 \quad (1)$$

$$\partial_t \phi_j + \nabla \cdot (\mathbf{v}_j \phi_j) = 0 \quad (2)$$

where  $\mathbf{v}_i(r)$  is the velocity of fluid  $i$  and  $\mathbf{v}_j(r)$  is the velocity of the solid material  $j$ .

Each velocity field may be split into two parts  $\mathbf{v}_i = \mathbf{v}_T + \mathbf{w}_i$ . The tube velocity  $\mathbf{v}_T = \sum_i \phi_i \mathbf{v}_i + \sum_j \phi_j \mathbf{v}_j$  represents the motion of the network of topological constraints in an entangled polymer melt as described in Brochard's theory of mutual diffusion [12], and  $\mathbf{w}_i$  represents the velocity of a given fluid relative to  $\mathbf{v}_T$ . The stress division parameters  $\alpha_i(r)$  and  $\beta_j(r)$  are obtained by balancing the frictional forces acting on the network as shown in [11].

The relative velocity fields are given by

$$\mathbf{w}_i = \frac{1}{\alpha_i} \nabla \phi_i - \frac{1}{\alpha_i} \nabla \phi_i + \frac{1}{\alpha_i} \nabla \phi_i + \frac{1}{\alpha_i} \nabla \phi_i \quad (3)$$

which are produced as a result of imbalanced osmotic forces  $\nabla \phi_i$ , pressure gradients  $\nabla p$ , viscoelastic forces  $\nabla \cdot \mathbf{T}$ , and external body forces  $\mathbf{f}$ . The relative velocity of each fluid is inversely proportional to its friction coefficient  $\alpha_i = \frac{1}{v_0} \phi_i N_e \zeta_i$  where  $\phi_i$  is the monomer friction coefficient of material  $i$  and  $v_0$  is the volume occupied by a single monomer.

The local force imposed on the fluid by each solid object is

$$\mathbf{f}_j(r) = \phi_j \nabla \phi_j + \phi_j \nabla p - \phi_j \nabla \cdot \mathbf{T} + \phi_j (\mathbf{v}_j - \mathbf{v}_T) \quad (4)$$

In the case where the wall velocities  $\mathbf{v}_j$  are specified, we may integrate over  $\mathbf{f}_j(r)$  to obtain the net force and net torque on each object, potentially enabling numerical rheometric experiments.

In the limit of low Reynolds number, the inertial terms may be neglected, and the momentum transport equation becomes a force balance equation.

$$0 = \nabla \cdot \mathbf{T} + \nabla p - \nabla \cdot \mathbf{T} + \mathbf{f} \quad (5)$$

This equation implicitly determines the mean velocity field  $\mathbf{v} = \sum_i \phi_i \mathbf{v}_i + \sum_j \phi_j \mathbf{v}_j$  which balances the net osmotic force  $\nabla \phi = \sum_i \phi_i \nabla \phi_i + \sum_j \phi_j \nabla \phi_j$ , the pressure gradient  $\nabla p$ , the viscoelastic forces  $\nabla \cdot \mathbf{T}$ , the net wall force  $\mathbf{f}$ , and the net body force acting on the fluid  $\mathbf{f}$ .

Energy is dissipated in the system by each of the terms in the dissipation functional  $\dot{W}$  [11], including friction due to the motion of each fluid relative to the polymer network  $\sum_i (\mathbf{v}_i - \mathbf{v}_T)$ , friction between the fluid and the walls  $\sum_j (\mathbf{v}_j - \mathbf{v}_T)$ , and elastic deformation of the polymer network  $\nabla \cdot \mathbf{T}$ . Note that in the absence of viscoelastic effects, the quantity  $\nabla \cdot \mathbf{T}$  reduces to the usual viscous dissipation term  $\nabla \cdot \mathbf{T}^2$ .

The mean velocity  $\mathbf{v}$  and pressure fields  $p$  must simultaneously satisfy the force balance condition Eq. (5) and the mass conservation condition,  $\nabla \cdot \mathbf{v} = 0$ . These relationships are not easily inverted and are obtained using an iterative numerical procedure. Once  $\mathbf{v}$  and  $w_j$  are known, the tube velocity may be calculated using the relationship

$$\mathbf{v}_T = \frac{\sum_i \phi_i (\mathbf{v}_i - \mathbf{v}_T) + \sum_j \phi_j (\mathbf{v}_j - \mathbf{v}_T)}{1 - \sum_i \phi_i} \quad (6)$$

Constitutive equations (7) and (8) are required to measure the bulk elastic stresses  $\mathbf{s}_i$  and shear elastic stresses  $\mathbf{s}_i$  induced by deformations of each entangled polymeric component.

$$\mathbf{s}_i = G_i \mathbf{T} \quad (7)$$

$$\mathbf{s}_i = K_i(r) \mathbf{T} \quad (8)$$

Although there are many possible constitutive equations, we have chosen to employ the Oldroyd-B model in which the total viscoelastic force is produced by the sum of the elastic forces contributed by each polymeric component and a dissipative viscous force,  $\nabla \cdot \mathbf{T} = \sum_i (\mathbf{s}_i + \mathbf{s}_i) + \mathbf{s}_i \nabla \cdot \mathbf{v}_T$ . This model allows us to study a purely viscous fluid ( $G_i = K_i = 0$ ), a purely viscoelastic melt ( $\mathbf{s}_i = 0$ ), or anything in-between. The derivatives in (7) and (8) are upper convected time derivatives,  $\overset{\circ}{\mathbf{T}} = \partial_t \mathbf{T} + \mathbf{v}_T \cdot \nabla \mathbf{T} - \mathbf{T} \cdot \nabla \mathbf{v}_T$ , and the shear strain rate tensor is  $\dot{\gamma}_{ij} = \partial_i v_{Tj} + \partial_j v_{Ti} - \frac{2}{d} (\mathbf{v}_T \cdot \nabla)_{ij}$ . The concentration dependent bulk moduli  $K_i$  and shear moduli  $G_i$  measure the stresses imposed on each component by the applied strains. Following Tanaka's example [9], we employ moduli of the form  $G_i(\phi) = G_{0i} \phi_i^2$  and  $K_i(\phi) = K_{0i} (\phi_i - f_i)$  where  $\phi_i$  is the step function. The quantity  $\tau_i$  represents the reptative disentanglement time associated with the characteristic entanglement length  $N_e$  of copolymer  $i$ . For simulations

with large elastic strains, this constitutive equation may be replaced with a more sophisticated phenomenological model or one based upon the SCFT microphysics [13].

A self-consistent calculation produces the chemical potential gradients which drive phase separation. The free energy of the melt is  $F = U - TS$  where the enthalpy is given by

$$U = kT = \frac{1}{v_0 N} \int d\mathbf{r} \left[ \frac{1}{2} \sum_{i,j} \chi_{ij} \phi_i \phi_j + \sum_{i,j} \chi_{ij} \phi_i \phi_j \right] \quad (9)$$

The  $\chi_{ij}$  and  $\chi_{ij}$  denote segment-segment and segment-wall interactions, respectively, and the entropy is

$$S = k \sum_i \phi_i \ln Q_i + \frac{1}{v_0 N} \int d\mathbf{r} \sum_i \phi_i \ln \phi_i \quad (10)$$

The quantity  $Q_i$  is the partition function over all configurations of a single copolymer species in the presence of the fields  $\phi_i$ .

Dynamic SCFT methods postulate that the system variables may be divided into two sets which relax on widely separated time scales. A "slow" set of parameters includes the elastic stresses and the conserved fields, mass, momentum, and monomer number. The remaining variables, including the conjugate chemical fields  $\phi_i$  are "fast" parameters, which satisfy the local thermodynamic equilibrium (LTE) conditions  $\delta F / \delta \phi_i = 0$  [13], which are derived by extremizing the free energy with respect to the conjugate fields  $\phi_i(\mathbf{r})$ . The non-equilibrium volume fraction fields  $\phi_i$  and  $\phi_j$  give rise to imbalanced chemical potentials  $\mu_i(\mathbf{r}) = \frac{\delta F}{\delta \phi_i(\mathbf{r})} = \frac{kT}{N v_0} \sum_j \chi_{ij} \phi_j + \chi_{ik} \phi_k \phi_i$  and  $\mu_j(\mathbf{r}) = \frac{\delta F}{\delta \phi_j(\mathbf{r})} = \frac{kT}{N v_0} \sum_i \chi_{ji} \phi_i + \chi_{jk} \phi_k \phi_j$  which drive diffusion and phase separation.

Calculations are performed in a periodic cell in two or three dimensions in which non-periodic geometries may be constructed using rigid materials. Spatial derivatives are computed pseudo-spectrally in Fourier space which enables the resolution of sharp domain interfaces with a small number of grid points and lends itself readily to parallelization. The multi-fluid model is solved iteratively for the  $\phi, w, f, v$  and  $p$  fields. Updated pressure and velocity fields are obtained from a projection method and frictional forces penalize flow relative to the walls. The method repeats until a pseudo-steady state is achieved which satisfies the no-flow, no-slip, continuity, and force balance conditions (5). The new velocity fields are then used to transport the volume fraction fields. Similarly, the local thermodynamic equilibrium conditions are solved by the iterative application of a hill climbing technique.

For concreteness, we have chosen to illustrate the technique by examining a single representative system in detail, namely the phase separation of a quenched triblock

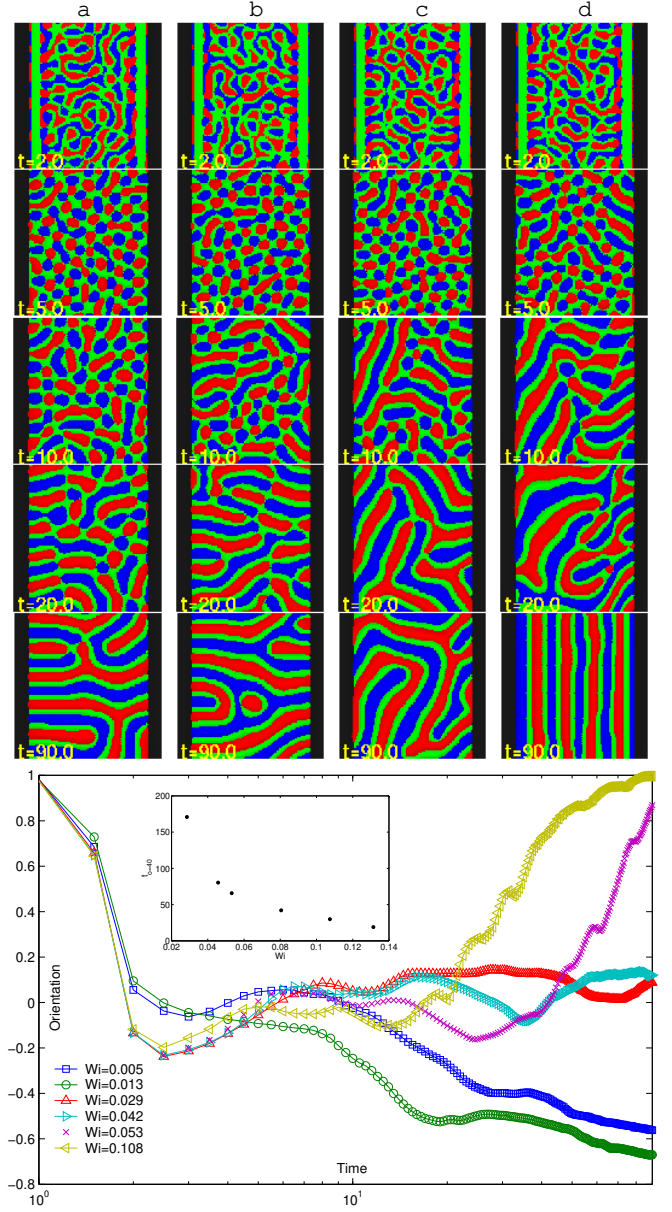


FIG. 1: [top] Time evolution of a quenched triblock melt in a sub-micron channel at several flow rates as characterized by the dimensionless Weissenberg number. (a)  $Wi = 0.005$  (b)  $Wi = 0.013$  (c)  $Wi = 0.029$  (d)  $Wi = 0.108$  [bottom] Lamellae orientation vs. time. The inset shows that time required to achieve  $O_{xy} = 0.40$  diverges as the Weissenberg number approaches  $Wi = 0.02$ .

copolymer melt in a sub-micron channel. The system consists of an incompressible melt of a symmetric ABC triblock copolymers ( $f_i = 1/3$ ) quenched from a disordered state into the intermediate segregation regime, in a channel of diameter  $D = 21R_g$ . The Flory incompatibility parameters are fixed at  $\chi = 25$ , and  $\chi = 12$  and all remaining parameters were chosen to approximate a polystyrene melt, with  $\eta_0 = 10^{-8}$  Ns/m and

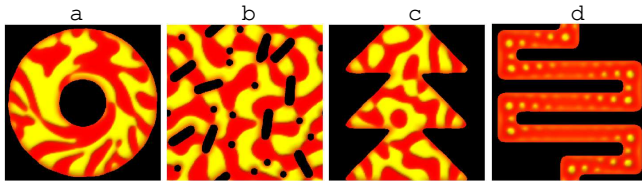


FIG. 2: Examples of 2D HSCFT systems: (a) A homopolymer blend A+B in two concentric, rotating cylinders (b) Nano-rods and nano-spheres in a phase separating blend (c) Viscoelastic flow of a blend through a microfluidic rectifier (d) A non-critical diblock ( $f = 0.3$ ) in a micro-reactor channel.

$G_0 = 2000\text{kPa}$  [14]. The flow rate is characterized by the dimensionless Weissenberg number  $Wi = \dot{\gamma}_{\text{max}} \dot{\gamma} D$  where  $\dot{\gamma}_{\text{max}}$  is the maximum mean velocity.

The images in Fig. 1 illustrate the morphology as a function of time at various Weissenberg numbers, where solid material is black and the copolymer blocks are red (A), green (B), and blue (C) respectively. We observe two distinct steady state configurations consisting of wall parallel and wall perpendicular lamellae, as illustrated by sequences (a) and (d) at  $t = 90$ . In the absence of flow, boundary wetting conditions dominate, resulting in a perpendicular orientation, and at high flow rates shearing effects dominate, resulting in a parallel orientation with blocks arranged in a CBA ABC configuration. The two effects compete, and we anticipate that there is some minimum Weissenberg number  $Wi_c$  required to achieve a wall parallel configuration.

To quantify these observations, we construct an orientation parameter  $\alpha_{xy} = \langle \cos^2(\theta) \rangle = \langle \cos^2(\theta) \rangle / \langle \sin^2(\theta) \rangle$  which measures the scattering difference between the x and y directions in Fourier space, where  $\langle \cdot \rangle$  is the radially averaged scattering intensity. The orientation parameter is plotted as a function of time for several values of  $Wi$  in Fig. 1, where  $\alpha_{xy} = 1$  corresponds to wall-parallel lamellae and  $\alpha_{xy} = 0$  corresponds to the wall-perpendicular conformation.

We estimate the value of the critical Weissenberg number,  $Wi_c$ , by plotting the time needed to achieve a parallel orientation, defined by  $\alpha_{xy}(t) > 0.40$ , as illustrated by the inset in Fig. 1. It is clear from the figure that the alignment time diverges near the critical Weissenberg number, allowing us to estimate  $Wi_c = 0.02$  in a channel of diameter  $D = 21R_g$ . Furthermore, by comparing the two slowest cases,  $Wi = 0.005$  and  $Wi = 0.013$ , we observe that a flowing melt with  $Wi > Wi_c$  approaches its steady state configuration more rapidly than a quiescent melt. Similarly, by comparing the  $Wi = 0.053$  and  $Wi = 0.108$  cases, we observe that a higher shear rate produces more rapid alignment in the  $Wi > Wi_c$  regime.

This numerical experiment also illustrates a type of dynamic asymmetry which arises in triblock copolymer melts. Although the system is compositionally symmetric,  $f_A = f_B = f_C$ , we see distinctly asymmetric struc-

tures in the early stages of phase separation as illustrated in Fig 1. At  $t = 1$ , we find wall parallel structures produced by preferential wetting of the walls by the A and C blocks, and at  $t = 5$ , we see an asymmetric drop-in-matrix morphology, indicating that early growth of density fluctuations is suppressed in regions which are enriched in block B segments. Since the enthalpic terms are all identical, we conclude that these effects are produced solely due to differences in the conformational entropy between the copolymer blocks. To our knowledge this type of dynamic asymmetry has not previously been discussed.

In addition to the example provided above, HSCFT is capable of modeling systems of far greater complexity. As illustrated in Fig. 2, some of the method's more unique capabilities include simulation of (a) the effects of moving machine parts on polymeric fluids (b) the unconstrained motion of solid nanoparticles (c) viscoelastic flow through irregular geometries and (d) flow in microfluidic channels.

In summary, we have developed a mesoscale technique which models the effects of viscoelastic, Navier-Stokes type hydrodynamic transport on inhomogeneous polymeric fluids in arbitrarily complex channels. In contrast with DSCFT methods, HSCFT is capable of describing the influence of moving machine elements, nontrivial pressure induced and drag induced velocity fields, and the unconstrained motion of solid nanoparticles. We believe this method has the potential for broad application and represents a first step toward more realistic simulations of complex fluid flows in industrial processing applications.

- 
- [1] G. H. Fredrickson, *The Equilibrium Theory of Inhomogeneous Polymers* (Oxford Press, 2006).
  - [2] F. D. rolet and G. H. Fredrickson, *Phys. Rev. Lett.* 83, 4317 (1999).
  - [3] G. H. Fredrickson, V. Ganesan, and F. D. rolet, *Macromolecules* 35, 16 (2002).
  - [4] J. G. E. M. F. et. al, *Journal of Chemical Physics*. 106, 4260 (1997).
  - [5] E. Reister, M. Muller, and K. Binder, *Physical Review E* 64, 41804 (2001).
  - [6] R. Hasegawa and M. Doi, *Macromolecules* 30, 3086 (1997).
  - [7] T. Kawakatsu, *Phys. Rev. E* 56, 3240 (1997).
  - [8] Y. Huo, H. Zhang, and Y. Yang, *Macromolecules* 36, 5383 (2003).
  - [9] H. Tanaka, *Phys. Rev. E* 56, 4451 (1997).
  - [10] T. Lo, M. Mihajlovic, Y. Shnidman, W. Li, and D. Gersappe, *Phys. Rev. E* 72, 040801 (2005).
  - [11] T. Taniguchi and A. Onuki, *Phys. Rev. Lett.* 77, 4910 (1996).
  - [12] F. Brochard, *Molecular Conformation and Dynamics of Macromolecules in Condensed Systems*, (Elsevier, 1988).
  - [13] G. Fredrickson, *Journal of Chemical Physics* 117, 6810 (2002).
  - [14] J. Merve, *Rheologica Acta* 43, 615 (2004).